

DSCC2015-9732

DISTRIBUTED FLOW SENSING USING BAYESIAN ESTIMATION FOR A FLEXIBLE FISH ROBOT

Feitian Zhang *

Department of Aerospace Engineering and
Institute for Systems Research
University of Maryland
College Park, MD, 20742
Email: fzhang17@umd.edu

Francis D. Lagor

**Derrick Yeo
Patrick Washington
Derek A. Paley**

Email: flagor@umd.edu, dyeo@umd.edu,
phw@terpmail.umd.edu, dpaley@umd.edu

ABSTRACT

Flexibility plays an important role in fish behaviors by enabling high maneuverability for predator avoidance and swimming in turbulence. In this paper, we present a novel, flexible fish robot equipped with distributed pressure sensors for flow sensing. The body of the robot is made of a soft, hyperelastic material that provides flexibility. The fish robot features a Joukowski-foil shape conducive to modeling the fluid analytically. A quasi-steady potential-flow model is adopted for real-time flow estimation, whereas a discrete-time vortex-shedding flow model is used for higher-fidelity simulation. The dynamics for the flexible fish robot are presented, and a reduced model for one-dimensional swimming is derived. A recursive Bayesian filter assimilates pressure measurements for estimating the flow speed, angle of attack, and foil camber. Simulation and experimental results are presented to show the effectiveness of the flow estimation algorithm.

INTRODUCTION

Fish have attracted scientific attention for their graceful locomotion, high maneuverability, and high energy efficiency. Inspired by nature, engineering researchers have made great efforts in designing and developing fish robots [1–5] that mimic real fish in order to improve the performance of underwater vehicles.

Fish robots are typically designed in two segments. The front segment holds the electronic components, including a bat-

tery, a micro-controller, navigational sensors, etc., whereas the back segment serves as the fish tail, usually flapped by a servo motor to provide thrust [3–5]. Although the multi-segment design is able to realize fish-like swimming motion by flapping the tail segment, the maneuverability achieved is still far less than real fish.

We know that flexibility plays an important role in fish behaviors by enabling high maneuverability for predator avoidance and swimming in turbulence. In this work, we describe a novel, flexible fish robot that deforms its body in a continuous way. The flexibility of the body is achieved by the property of the material of the robot, rather than the rotational links between rigid parts. In this paper, we choose silicone rubber for the material and select a Joukowski foil [6] for the shape. This choice of shape is conducive to modeling the fluid dynamics.

Flow sensing is important for fish to navigate in unknown, murky, and cluttered environments [7]. However, traditional submarines do not have this capability. Sonar is unsuitable for a fish robot due to its large cost, power consumption, and size [8]. Additionally, sonar may not provide accurate measurements at low speeds. Inertial measurement units (IMUs) accumulate errors over time due to dead reckoning [8]. In addition, IMUs do not provide information pertaining to the flow environment.

The lateral line is a flow-sensing organ that fish use to detect movement and vibration in the surrounding water [7]. The recent development of artificial lateral-line systems shows promise for the application of flow sensing to underwater robots [9, 10]. In our previous work, we studied rheotaxis (i.e., aligning up-

*Address all correspondence to this author.

stream [10]) with a steady, rigid Joukowski-shaped fish robot by estimating the flow field using an artificial lateral-line system made of distributed pressure sensors [9, 10]. In this work, we extend the previous research to a flexible Joukowski-shaped fish robot with one-dimensional, free-swimming dynamics.

This paper presents two flow models of a flexible, foil-shaped fish robot: a quasi-steady potential-flow model and a higher-fidelity vortex-shedding model. The quasi-steady potential-flow model is adopted for flow estimation due to its tractability, whereas the vortex-shedding model is used in simulation to generate the flow field as ground truth for testing the flow estimation algorithm. The deformation of the robot body is modeled using a time-varying parameter (the camber ratio). A recursive Bayesian filter assimilates the distributed pressure-sensor measurements. A testbed consisting of a flow tank, gantry system, and air-bearing linear guide is used to demonstrate one-dimensional swimming. The experimental results show the effectiveness of the flow-sensing algorithm during flapping motion of a flexible fish robot.

FLOW MODEL FOR A JOUKOWSKI-SHAPED FLEXIBLE FISH ROBOT

This paper adopts the shape of a Joukowski foil for the design of the fish robot in order to utilize potential-flow theory to model the flow field. In fluid dynamics, potential-flow theory [6] describes the velocity field of incompressible, irrotational flow as the gradient of a scalar function, the velocity potential. This section describes the two-dimensional flow past a cambered Joukowski foil, first using the quasi-steady potential-flow method and then using the unsteady vortex-shedding method.

Quasi-steady Potential-flow Model

The fish robot modeled as a Joukowski foil takes the shape of the output of the Joukowski transformation of a circle. The Joukowski transformation, which is essentially a conformal mapping, is expressed as [6]

$$z^0 = \xi + \frac{a^2}{\xi}, \quad (1)$$

where the set of points ξ represents a circle with radius R centered at ξ_0 in the complex ξ -plane, as shown in Fig. 1. The coordinate of the intersection of the circle and the x_ξ -axis is the Joukowski transformation parameter a , which is approximately one quarter of the chord length of the foil l . The image of the mapping in the z^0 -plane defines the boundary of the fish robot (Fig. 2). The origin of the z^0 -plane is O^0 . The x^0 -axis points along the chord line from the leading edge to the trailing edge.

Define the body-fixed frame (the z -plane) by translating the z^0 -plane from point O^0 to the point O , about which the fish robot

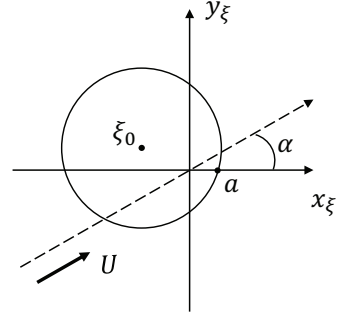


FIGURE 1: ξ -plane and coordinates.

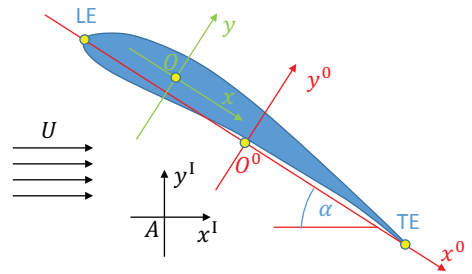


FIGURE 2: Illustration of reference frames A and O . TE is the trailing edge and LE is the leading edge.

flaps or rotates. The center of rotation for the flapping motion is chosen to be the one-quarter point along the camber line, as measured from the leading edge. Let z_O^0 be the coordinate of point O in the z^0 -plane. The transformation from the ξ -plane to the z -plane is

$$z = \xi + \frac{a^2}{\xi} - z_O^0. \quad (2)$$

A two-dimensional fluid with velocity U_f flows past the foil-shaped fish robot. The inertial frame is defined so that the incoming flow velocity U_f is aligned with the x^I -axis. The flow velocity relative to the body is denoted U . The angle between the x -axis and the direction of the relative velocity U is the angle of attack α , with the nose pitching up chosen to be the positive direction (Fig. 2).

There are three parameters that define the Joukowski shape in the ξ -plane: the radius of the circle R , the coordinate a of the intersection point on the x_ξ -axis, and the center of the circle ξ_0 . The geometric relationship of the three parameters obeys

$$R = |a - \xi_0|. \quad (3)$$

Assume that the circle radius R and the area of the Joukowski foil are constant during the flapping motion, even when the shape

changes. (This assumption is based on the incompressibility of the foil material.) The area of the Joukowski foil is [11]

$$S = \pi R^2 \left(1 - \frac{a^4}{(R^2 - |\xi_0|^2)^2} \right). \quad (4)$$

Parameter k describes the instantaneous shape of the fish robot,

$$k = \frac{a^2}{R^2 - |\xi_0|^2}. \quad (5)$$

Along with the constant R , the shape of the fish robot is determined by the placement of the circle center $\xi_0 = [x_{\xi_0}, y_{\xi_0}]$, as described next.

In the foil plane, there are two shape parameters for the Joukowski foil: the camber ratio H and the thickness ratio T [6]. Intuitively, the camber ratio describes how much the foil bends. Under the assumption that $|\xi_0| \ll a$, which is normally true for a moderately cambered Joukowski foil, H and T are linearly dependent on the vertical and horizontal displacement of the center of the circle, x_{ξ_0} and y_{ξ_0} , respectively, i.e.,

$$H = \frac{y_{\xi_0}}{2a}, \quad \text{and} \quad (6)$$

$$T = -\frac{3\sqrt{3}x_{\xi_0}}{4a}. \quad (7)$$

Assume that the flexible fish robot changes its shape while maintaining a cambered Joukowski foil profile, meaning that each state of the deformation corresponds to a Joukowski foil shape with instantaneous camber ratio H . (The camber ratio captures the degree of bending during the deformation.) Given a camber ratio H that corresponds to the swimming state of the fish robot, we calculate the following shape parameters in the ξ -plane:

$$y_{\xi_0} = \frac{4kRH}{((k+1)^2 + (4kH)^2)^{\frac{1}{2}}}, \quad (8)$$

$$x_{\xi_0} = \frac{k-1}{k+1} \left(R^2 - y_{\xi_0}^2 \right)^{\frac{1}{2}}, \quad \text{and} \quad (9)$$

$$a = \frac{2k}{k+1} \left(R^2 - y_{\xi_0}^2 \right)^{\frac{1}{2}}. \quad (10)$$

According to potential-flow theory [6], the flow in the circle plane (ξ -plane) generates the flow in the corresponding foil plane (z -plane), according to a conformal map. In an inviscid, incompressible, and irrotational fluid, the quasi-steady complex potential of the flow in the ξ -plane is a function of the relative

flow speed U , the angle of attack α , the radius R , and the center ξ_0 . The complex potential [6]

$$W(\xi) = U(\xi - \xi_0)e^{-i\alpha} + U \frac{R^2}{\xi - \xi_0} e^{i\alpha} + i \frac{\Gamma}{2\pi} \ln(\xi - \xi_0), \quad (11)$$

represents the sum of three elementary flow fields: a uniform flow, a doublet, and a point vortex located at the center of the circle. The vortex circulation Γ is evaluated by enforcing the Kutta condition [6], which requires the trailing edge to be a stagnation point. The vortex circulation is [6]

$$\Gamma = 4\pi R U \sin(\alpha + \beta). \quad (12)$$

Here $\beta = \arcsin(x_{\xi_0}/R) \approx 2H$ is the phase angle of the center point ξ_0 . Under the assumption that $|\xi_0| \ll a$, β is approximated by $2H$.

The conjugate flow velocity $\overline{f(z)} = u - iv$ in the z -plane (the overline notation $\overline{}$ denotes the conjugate operator) is calculated using the complex potential in the ξ -plane and the Joukowski transform function, which yields

$$\overline{f(z)} = \frac{\partial W}{\partial \xi} \left(\frac{\partial z}{\partial \xi} \right)^{-1}, \quad (13)$$

where ξ is obtained using the inverse Joukowski transform

$$\xi = \xi(z) = 0.5(z + z_0^0) \pm \sqrt{0.25(z + z_0^0)^2 - a^2}. \quad (14)$$

(The root outside the ξ -plane circle is used.) With the quasi-steady potential-flow model (13) and the shape-parameter relationship in the Joukowski transformation (8)–(10), we calculate the flow field around the fish robot foil, given any parameter set (U, α, H) .

Vortex-shedding Flow Model

The quasi-steady potential-flow model (13) does not describe the unsteady or transient effects caused by the flapping motion of a flexible fish robot. This subsection presents a second flow model, used for simulation, that features discrete-time vortex shedding. In this model, a new vortex is shed into the flow from the trailing edge of the foil at every discrete time step. The shed vortices convect with the flow according to the local fluid velocity. The net circulation around the robot body contributes to drag, which is not predicted by the quasi-steady potential-flow theory. The accuracy of the vortex-shedding method has been investigated and validated [11, 12]. However, the system complexity increases with time and grows too fast for real-time use. We

instead use the vortex-shedding method for simulating the flow field and to test the effectiveness of the quasi-steady potential-flow model for flow-parameter estimation.

Let Ω be the angular velocity of the fish robot with counter-clockwise rotation about the pivot point O chosen to be the positive direction ($\dot{\alpha} = -\Omega$). In the vortex-shedding model, the complex flow potential with respect to the ξ -plane is

$$W = U(\xi - \xi_0)e^{-i\alpha} + U\frac{R^2}{\xi - \xi_0}e^{i\alpha} + \Omega W_\Omega + i\frac{\Gamma_0}{2\pi} \ln \frac{\xi - \xi_0}{R} + \sum_{k=1}^n i\frac{\Gamma_k}{2\pi} \left(\ln(\xi - \xi_k) - \ln\left(\xi - \xi_0 - \frac{R^2}{\xi_k - \xi_0}\right) \right), \quad (15)$$

The corresponding complex potential is denoted by W_Ω . Γ_0 represents the vortex circulation at the center of the circle and Γ_k represents the circulation of the k^{th} vortex located at position ξ_k .

From the boundary condition, the unit complex potential for the rotation motion has the constraint [11]

$$\text{Im}\{W_\Omega\} = \text{Im}\left\{-i\frac{z\bar{z}}{2}\right\}. \quad (16)$$

The unit complex potential is

$$W_\Omega = -\frac{i}{2} \left(R^2 + 2\xi_0 \frac{R^2}{\xi - \xi_0} + |\xi_0|^2 + 2a^2 \frac{\frac{R^2}{\xi - \xi_0} + \bar{\xi}_0}{\xi} + 2z_0^0 \frac{R^2}{\xi} + 2\bar{z}_0^0 \left(\xi_0 + \frac{a^2}{\xi} \right) + z_0^0 \bar{z}_0^0 + \frac{a^4(\xi - 2\xi_0)}{\xi(R^2 - |\xi_0|^2)} \right). \quad (17)$$

The complex velocity in the z -plane using the vortex-shedding method is

$$\overline{f(z)} = \frac{\partial W}{\partial \xi} \left(\frac{\partial z}{\partial \xi} \right)^{-1}. \quad (18)$$

The above equation describes the entire flow field, except at the vortex locations, which are singular points and thus undefined. Using Routh's rule [13], the k^{th} vortex conjugate velocity $\overline{f(z_k)} = u_{z_k} - iv_{z_k}$ is

$$\begin{aligned} \overline{f(z_k)} &= \frac{d\bar{z}_k}{dt} = \frac{d}{dz} \left(W - i\frac{\Gamma_k}{2\pi} \ln(z - z_k) \right) \Big|_{z=z_k} \\ &= \left(\frac{dz}{d\xi} \right)^{-1} \frac{d}{d\xi} \left(W(\xi) - i\frac{\Gamma_k}{2\pi} \ln(\xi - \xi_k) \right) \\ &\quad - i\frac{\Gamma_k}{4\pi} \frac{d^2 z}{d\xi^2} \left(\frac{dz}{d\xi} \right)^{-2} \Big|_{\xi=\xi_k}. \end{aligned} \quad (19)$$

The circulation strength Γ_k of the vortex shed into the flow at the point ξ_k is evaluated by enforcing the Kutta condition at the trailing edge, which requires

$$\frac{\partial W}{\partial \xi} \Big|_{\xi=a} = 0. \quad (20)$$

The position of the shed vortex z_k may be modeled using one of several existing approaches. This paper adopts the "1/3 arc-length" method introduced by Streitlien and Triantafyllou [13], which places the shed vortex at the one-third point of the arc tangent to the camber line at the trailing edge and passing through the previous vortex point. Thus,

$$z_k = (z_{k-1} - z_{\text{TE}}) \frac{1 - e^{i\theta/3}}{1 - e^{i\theta}} = \frac{z_{k-1} - z_{\text{TE}}}{1 + e^{i\frac{\theta}{3}} + e^{i\frac{2\theta}{3}}} + z_{\text{TE}}. \quad (21)$$

Here the trailing-edge coordinate is $z_{\text{TE}} = 2a - z_0^0$ and θ is the arc angle satisfying

$$e^{i\theta} = e^{-i2(-2\beta)} \frac{(z_{k-1} - z_{\text{TE}})^2}{|z_{k-1} - z_{\text{TE}}|^2}, \quad (22)$$

where $\beta = \arcsin(y_{\xi_0}/R)$ as before.

When the fish robot rotates about the point O , the z -reference frame also rotates with it, whereas the shed vortices move as predicted by Routh's rule in the inertial frame. Therefore, the vortex coordinates with respect to the z -plane are

$$z_k(N+1) = (z_k(N) + f(z_k)T)e^{i\Delta\alpha}, \quad (23)$$

where $z_k(N)$ is the k^{th} vortex coordinate in the z -plane at the N^{th} time step, T is the time step, and $\Delta\alpha$ is the change in the angle of attack from the N^{th} time step to the $(N+1)^{\text{th}}$ time step.

DYNAMIC MODEL OF A FLEXIBLE FISH ROBOT

This section presents a dynamic model of a flexible fish robot with hydrodynamic and thrust forces. Let $\mathbf{\Pi} = \mathbf{J}\omega$ and $\mathbf{P} = \mathbf{M}\mathbf{v}$ denote the total angular and linear momenta of the robot-fluid system, respectively, where ω is the angular velocity of the body-fixed frame with respect to the inertial frame expressed in the body-fixed frame, \mathbf{v} is the corresponding translational velocity, \mathbf{J} is the inertia matrix, and \mathbf{M} is the mass matrix. Both \mathbf{J} and \mathbf{M} include the added-mass effect from water acting on the fish robot during acceleration or deceleration. Assume the off-diagonal terms in the inertia matrix are negligible and the added

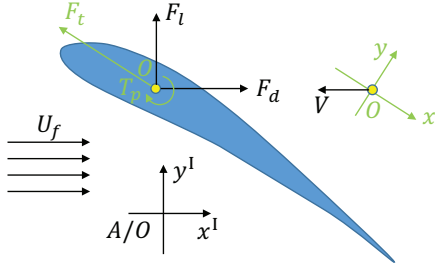


FIGURE 3: Schematic of hydrodynamic forces and moments.

mass and added inertia do not vary significantly during the flapping motion. The dynamics of the fish robot are governed by Kirchhoff's equations [14], i.e.,

$$\dot{\mathbf{\Pi}} = \mathbf{\Pi} \times \boldsymbol{\omega} + \mathbf{P} \times \mathbf{v} + \mathbf{T} \quad (24)$$

$$\dot{\mathbf{P}} = \mathbf{P} \times \boldsymbol{\omega} + \mathbf{F}, \quad (25)$$

where \mathbf{T} is the external moment vector and \mathbf{F} is the external force vector.

For the planar motion of the fish robot, which is the focus of this paper, we have

$$\boldsymbol{\omega} = [0, 0, \Omega]^T, \quad \mathbf{v} = [v_1, v_2, 0]^T, \quad \mathbf{\Pi} = [0, 0, J\Omega]^T,$$

$$\mathbf{P} = [m_1 v_1, m_2 v_2, 0]^T, \quad \mathbf{T} = [0, 0, T_p]^T,$$

$$\text{and } \mathbf{F} = [-(F_t - F_d \cos \alpha + F_l \sin \alpha), F_l \cos \alpha + F_d \sin \alpha, 0]^T.$$

Here J is the sum of the inertia of the robot and the added inertia in the pitching direction, and m_1 and m_2 are the sum of the mass of the robot and the added mass in the surge and sway directions, respectively. Figure 3 illustrates the hydrodynamic pitching torque T_p , the thrust force F_t , generated by the flapping motion of the foil with the $-x$ -axis direction as positive, the drag force F_d , in the opposite direction of the motion of the robot relative to the fluid, and the lift force F_l , perpendicular to the relative-flow direction.

The hydrodynamic forces and moment are modeled following aerospace engineering conventions [15], i.e.,

$$T_p = C_p(\alpha + 2H)U^2 - K_p\Omega \quad (26)$$

$$F_d = (C_d^0 + C_d(\alpha + 2H)^2)U^2 \quad (27)$$

$$F_l = C_l(\alpha + 2H)U^2, \quad (28)$$

where C_p , C_d^0 , C_d , and C_l are hydrodynamic coefficients that can be identified using flow-tunnel experiments, and K_p is the pitch damping coefficient.

Selecting a sinusoidal waveform for the angle-of-attack implies

$$\alpha = A \sin \phi = A \sin(2\pi f t), \quad (29)$$

where ϕ is the phase angle of the angle of attack, and A and f represent the amplitude and frequency of the periodic control input α , respectively. The thrust force generated by the periodic actuation (29) is approximated as [3]

$$F_t = \bar{F}_t + (\hat{F}_t - \bar{F}_t) \sin(2\phi), \quad (30)$$

where \bar{F}_t and \hat{F}_t are the mean and maximum thrust force in one flapping period, respectively. The mean and maximum thrust force depend on the product of the amplitude and frequency of the flapping motion [3], i.e.,

$$\bar{F}_t = k_1(Af)^{k_2} \quad (31)$$

$$\hat{F}_t = k_3(Af)^{k_4}. \quad (32)$$

The parameters k_1 , k_2 , k_3 , and k_4 are identified by force-sensing experiments (k_2 and k_4 are approximately equal to 2 [3]).

Define V as the speed of the fish robot with respect to the inertial frame, with the $-x^I$ -axis direction as positive. The inertial flow speed along the x^I -axis is U_f . Therefore, the relative speed of the flow with respect to the robot is $U = U_f + V$. We also have $v_1 = -V \cos \alpha$ and $v_2 = -V \sin \alpha$.

This paper focuses on one-dimensional swimming. The robot moves only along the x^I -axis and the angle of attack is directly controlled, so the dynamics become

$$\begin{aligned} -m_1 m_2 \dot{U} &= (m_1^2 - m_2^2)(U - U_f)\Omega \sin \alpha \cos \alpha \\ &\quad - (F_t - F_d \cos \alpha + F_l \sin \alpha)m_2 \cos \alpha \\ &\quad + (F_l \cos \alpha + F_d \sin \alpha)m_1 \sin \alpha. \end{aligned} \quad (33)$$

Modeling camber dynamics is a challenging fluid-structure-interaction problem that may involve continuum mechanics and boundary-value partial differential equations. However, we use a tractable model to capture the camber motion for the purpose of real-time control. The camber kinematics are a linear function of the second derivative of the angle of attack with respect to time, i.e.,

$$\dot{H} = -K_h \ddot{\alpha} = K_h \dot{\Omega}, \quad (34)$$

where K_h is the camber-dynamics coefficient.

FLOW ESTIMATION USING BAYESIAN FILTER WITH DISTRIBUTED PRESSURE SENSORS

Flow estimation for underwater robots is a challenging problem, especially for low-speed operations. This section describes a distributed flow-sensing algorithm using a Bayesian filter. The algorithm assimilates distributed pressure measurements to estimate the relative flow speed U for real-time use. The Bayesian filter also estimates the angle of attack α and the camber ratio H for the flexible foil, unlike our previous paper [10], which only estimated relative flow speed and angle of attack for a rigid foil.

Consider a flexible fish robot equipped with N_p pressure sensors located at positions $z_{p_i}, i = 1, \dots, N_p$. Each pressure sensor measures the local static pressure modeled by the Bernoulli's equations for inviscid, incompressible flow along a streamline [6]

$$p_i = C - \rho \frac{\partial \phi(z_{p_i})}{\partial t} - \frac{1}{2} \rho |f(z_{p_i})|^2, \quad (35)$$

where p_i is the predicted static pressure at location z_{p_i} , $f(z_{p_i})$ is the local flow velocity, ρ is the water density, and C is a constant. $\phi = (W + \overline{W})/2$ is the time-dependent velocity potential.

Inspired by the lateral-line system in fish [7], the pressure differences between each sensor pair form the individual flow measurement of the fish robot. The flow measurement equation is [9, 10]

$$\begin{aligned} \Delta p_{ij} &= p_i - p_j \\ &= \frac{1}{2} \rho (|f(z_{p_j})|^2 - |f(z_{p_i})|^2) + \frac{1}{2} \rho \left(\frac{\partial \phi(z_{p_j})}{\partial t} - \frac{\partial \phi(z_{p_i})}{\partial t} \right). \end{aligned} \quad (36)$$

There are $N_m = (N_p)!/2!/(N_p - 2)!$ possible measurements in total, i.e., the combinatorial number of sensor pairs. We assume a quasi-steady flow for estimation purposes, meaning there is no unsteady effect, i.e.,

$$\frac{1}{2} \rho \left(\frac{\partial \phi(z_{p_j})}{\partial t} - \frac{\partial \phi(z_{p_i})}{\partial t} \right) = 0 \quad (37)$$

Define $\mathbf{z}_p = [z_1, \dots, z_{N_p}]^T$ and $\Delta \mathbf{p} = [\Delta p_{12}, \dots, \Delta p_{1N_p}, \Delta p_{23}, \dots, \Delta p_{2N_p}, \dots, \Delta p_{N_p-1N_p}]^T$ as the vectors representing sensor locations and flow measurements, respectively. Assuming the flow measurements of the fish robot $\Delta \mathbf{p}$ are corrupted with Gaussian noise, then the actual i th element of the measurement vector is

$$\Delta \tilde{\mathbf{p}}(i) = \Delta \mathbf{p}(i) + \eta_i, \quad (38)$$

where $\eta_i \sim N(0, \sigma_i^2)$ is drawn from a zero-mean Gaussian distribution with variance σ_i . Here the Gaussian distribution of the flow measurement is based on the assumption that the pressure sensor output is corrupted with Gaussian noise and the fact that the summation of two Gaussian variables is also Gaussian.

Given the pressure-difference measurements, we need a flow model for the flapping fish robot to reconstruct the flow field. Although the vortex-shedding model (18) is a reliable model for describing flow field, the discrete-time vortex addition is not suitable for real-time estimation. A more tractable model is needed to approximate the flow field and to help estimate the motion of the robot, so we adopt the quasi-steady potential-flow model (13). Let $\mathbf{\Lambda} = [U, \alpha, H]^T$ represent the flow parameter vector. We use the Bayesian filter to estimate $\mathbf{\Lambda}$ based on distributed flow measurements.

The Bayesian filter, also known as recursive Bayesian estimation [16], is a general probabilistic approach for estimating an unknown probability density function (pdf) recursively over time using incoming measurements and a mathematical process model. In this work, the flow measurements $\Delta \tilde{\mathbf{p}}$ are assimilated recursively at each step to infer the most likely parameter vector $\hat{\mathbf{\Lambda}}$. The Bayesian formula for calculating the posterior probability of the flow parameters from the acquired measurements is [16]

$$p(\mathbf{\Lambda}(t) | \mathbf{D}(t)) = \kappa p(\Delta \tilde{\mathbf{p}} | \mathbf{\Lambda}) p(\mathbf{\Lambda}(t) | \mathbf{D}(t - \Delta t)), \quad (39)$$

where $p(\Delta \tilde{\mathbf{p}} | \mathbf{\Lambda})$ is the likelihood function of the new measurements $\Delta \tilde{\mathbf{p}}$ given the parameters $\mathbf{\Lambda}$, $p(\mathbf{\Lambda}(t) | \mathbf{D}(t))$ and $p(\mathbf{\Lambda}(t) | \mathbf{D}(t - \Delta t))$ are the posterior and prior pdf for time t , respectively, $\mathbf{D}(t) = \{\Delta \tilde{\mathbf{p}}(t), \Delta \tilde{\mathbf{p}}(t - \Delta t), \dots, \Delta \tilde{\mathbf{p}}(0)\}$ represents all pressure difference measurements up to time t , and κ is the coefficient that ensures the total probability of the posterior over the parameter space is equal to 1. This paper uses a grid-based Bayesian filter to discretize the parameter space, because it is easier to implement than a particle filter.

The assumption of Gaussian noise in the flow measurements leads to a Gaussian likelihood function,

$$p(\Delta \tilde{\mathbf{p}}(i) | \mathbf{\Lambda}) = \frac{1}{\sqrt{2\pi}\sigma_i} \exp\left(-\frac{1}{2\sigma_i^2} (\Delta \mathbf{p}(i) - \Delta \tilde{\mathbf{p}}(i))^2\right), \quad (40)$$

where $i = 1, \dots, N_m$ is the index for the i th element of the pressure measurement vector $\Delta \tilde{\mathbf{p}}$.

The prior pdf $p(\mathbf{\Lambda}(t) | \mathbf{D}(t - \Delta t))$ is generated from the posterior $p(\mathbf{\Lambda}(t - \Delta t) | \mathbf{D}(t - \Delta t))$ calculated at time $t - \Delta t$; the initial condition of the prior probability $p(\mathbf{\Lambda}(0) | \mathbf{D}(-\Delta t))$ is a uniform distribution. The prior updated by the Chapman-Kolmogorov

TABLE 1: Parameters used in simulation for the flexible fish robot.

Parameter	Value	Parameter	Value
m_1	1.0 kg	m_2	1.5 kg
C_{D0}	30 kg·m ⁻¹	C_D	100 kg·m ⁻¹
C_L	10 kg·m ⁻¹	K_H	0.1
k_1	49.6 kg·m	k_2	2
k_3	87.6 kg·m	k_4	2

equation [16] is

$$\begin{aligned}
 & p(\mathbf{\Lambda}(t)|\mathbf{D}(t-\Delta t)) \\
 &= \int p(\mathbf{\Lambda}(t)|\mathbf{\Lambda}(t-\Delta t))p(\mathbf{\Lambda}(t-\Delta t)|\mathbf{D}(t-\Delta t))d\mathbf{\Lambda}(t-\Delta t),
 \end{aligned}
 \tag{41}$$

where $p(\mathbf{\Lambda}(t)|\mathbf{\Lambda}(t-\Delta t))$ represents the time evolution of the probability density function of the motion. In this paper, we use a normal distribution to model the probability density diffusion over time, i.e.,

$$p(\mathbf{\Lambda}(t)|\mathbf{\Lambda}(t-\Delta t)) \sim N(g(\mathbf{\Lambda}(t-\Delta t)), \Sigma_p), \tag{42}$$

where $g(\mathbf{\Lambda})$ is the time-evolution function of estimation parameters governed by the dynamic model (33)–(34) and Σ_p is the process variance matrix.

SIMULATION OF FLOW ESTIMATION

Simulations are used to evaluate the distributed flow-sensing algorithm. We simulate flow estimation during a sinusoidal control input with constant amplitude. The simulated flow field is generated from the vortex-shedding model (18). The fish dynamics are simulated using the motion model (33)–(34). Values for the coefficients of the hydrodynamic model were obtained experimentally using the setup described in the experiment section. Six pressure sensors are distributed on each side of the fish robot, which measures 20 cm in total, with a distance along the center line of 2.5 cm, 7.5 cm, and 10 cm from the leading edge. The inertial flow speed is set to 20 cm/s. The flapping actuation frequency and amplitude in simulation are 0.75 Hz and 15°, respectively. The remaining parameters used in simulating the flexible fish robot are shown in Table 1.

Figure 4 shows snapshots of the flapping fish robot in a uniform flow field. A vortex is introduced at each time step to capture the unsteady effect of the flow. The Bayesian estimation results are shown in Fig. 5. The speed estimate is accurate, whereas the angle-of-attack estimate has a phase lead over

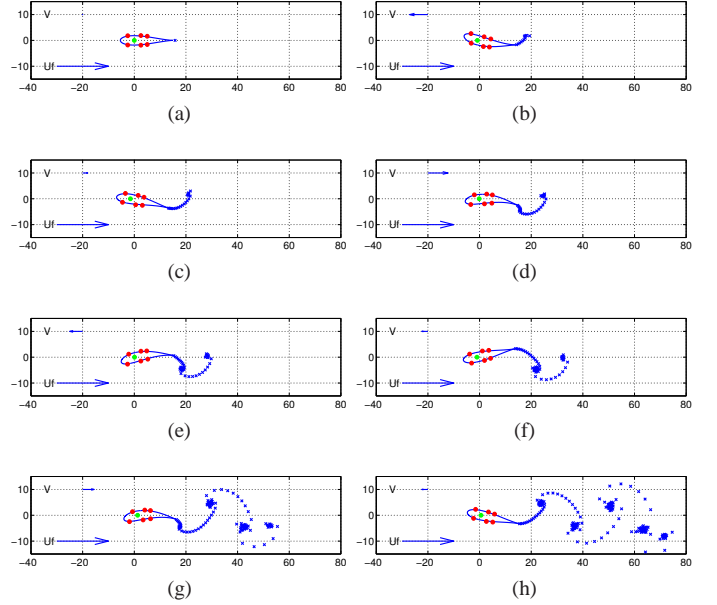


FIGURE 4: Snapshots of unidirectional swimming of the fish robot using the vortex-shedding method. (a) $t = 0$ s; (b) $t = 0.2$ s; (c) $t = 0.4$ s; (d) $t = 0.6$ s; (e) $t = 0.8$ s; (f) $t = 1$ s; (g) $t = 2$ s; (h) $t = 3$ s. V is the the swimming speed of the robot with respect to the inertial frame and U_f is the uniform flow speed with respect to the inertial frame.

the actual waveform. Also, the amplitude of the camber ratio is overestimated, perhaps from using a simplified flow model in the Bayesian estimation. However, for the purpose of swimming-profile control, such as rheotaxis or speed regulation, we need the “mean” motion of the fish robot, or the average of the angle of attack and relative flow speed over one period of flapping actuation. Based on the simulation results, the quasi-steady flow model used in the Bayesian filter provides a satisfactory estimate of the flow field despite its simplicity.

EXPERIMENTAL RESULTS FOR FLOW ESTIMATION

This section presents the experimental design and results for evaluating the flow-sensing algorithm for a flexible fish robot. We first discuss the fabrication of a flexible fish robot, and then introduce the design of the experimental testbed. The experimental results for flow sensing are presented to demonstrate the effectiveness of the flow estimation algorithm.

Experimental Setup

We chose silicone rubber (Ecoflex 00-30 from Smooth-On) as the flexible material for the fish robot. Cured rubber is soft and strong with Shore 00-30 hardness. We first designed a mold of the fish robot in SolidWorks, as shown in Figs. 6a and 6b, and

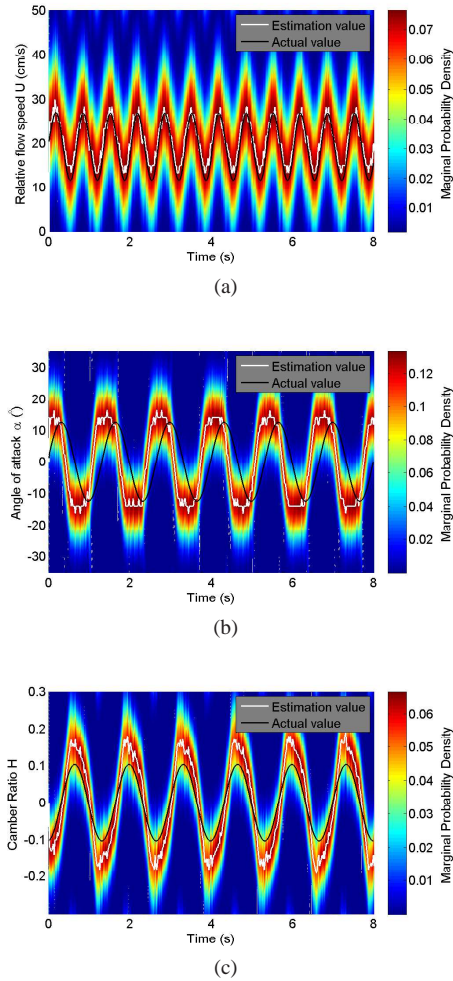


FIGURE 5: Marginal probability densities for the states of the Bayesian filter in the flow-sensing simulation: (a) the relative flow speed U ; (b) the angle of attack α ; and (c) the camber ratio H .

then manufactured the mold using a high-precision 3D printer. We poured the mixed silicone rubber compound into the mold and then kept it in a vacuum chamber during curing to avoid bubbles. For actuation of the angle of attack, a mini shaft from MakerBeam was inserted before the molding process at the one-quarter-point of the chord, behind the leading edge. For the pressure sensor ports, holes of radius 1 mm were placed on each side of the mold at a distance along the center line of 2.5 cm, 7.5 cm, and 10 cm behind the leading edge. We packaged six pressure sensors (Servoflo MS5401-BM) with appropriately sized tubing, and fixed the sensors to the center shaft. Each pressure sensor outputs analog voltage in proportion to the local pressure. The whole fish robot measures 20 cm long, 3.6 cm wide, and 12 cm tall as shown in Fig. 6c.

The experimental testbed for holding the fish robot and guid-

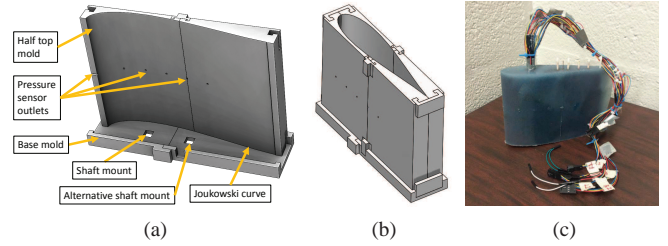


FIGURE 6: Illustration of the molding design for the fish robot: (a) mold interior; (b) mold assembly; and (c) the fish robot after molding.

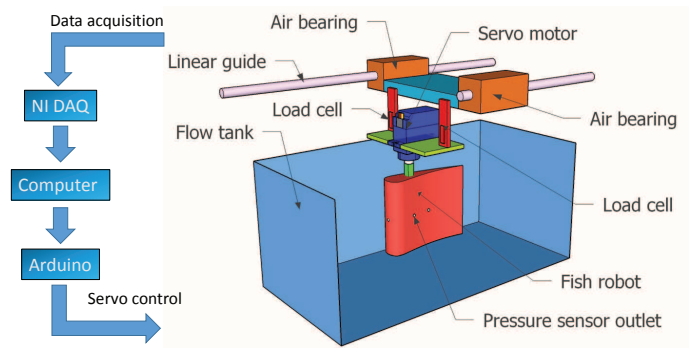


FIGURE 7: Schematic of the testbed.

ing the motion was designed to facilitate the flow-sensing experiment; a schematic is shown in Fig. 7. A double-rail linear guide is mounted to a 80/20 frame. We used two linear motion air bearings (NEWWAY porous air bearing) to allow for low-friction horizontal motion. A gantry platform was mounted on those bearings to support the fish robot. Two load cell sensors (300 g measurement range) mounted vertically at equal distance from the center detect the force and torque in the surge and pitching directions, respectively. A DC servo (Savox 0235MG) sits between the two load cells. The servo arm is bolted to an L-shape MakerBeam rigidly attached to the fish to control the angle of attack. This setup was used for water-tunnel experiments to identify the hydrodynamic coefficients in Table 1, and to investigate the thrust-force generation from the periodic flapping motion [3]. When the air bearing is turned on, the fish robot moves freely along the guiding rail. The entire test platform is placed over a Loligo 185 L flow tank, which generates a uniform flow field within an enclosed test section that measures $25 \times 25 \times 87.5$ cm, as shown in Fig. 8.

Flow-sensing Experiments

This subsection presents results from testing the recursive Bayesian estimation algorithm during one-dimensional swimming. The fish robot is still for the first 5 seconds, and then

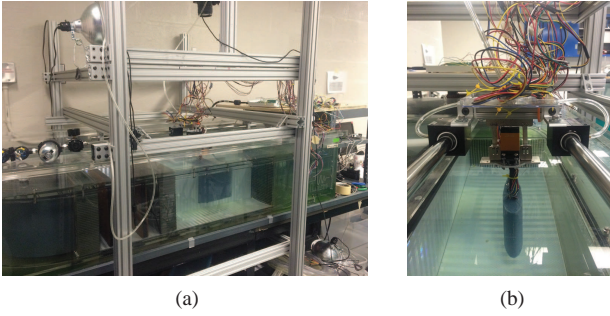


FIGURE 8: The experimental setup. (a) Side view; (b) front view.

flaps for 10 seconds. The angle-of-attack actuation signal is sinusoidal with a frequency of 0.75 Hz and a constant amplitude of 10° . The uniform flow speed is 18.74 cm/s, which is calibrated using a OTT MF-Pro flow meter. The air bearing operates throughout the experiment to allow the fish to move forward and backward. The measurement data is acquired from the pressure sensors using DAQ 6225 from National Instruments. The data is then transmitted via USB to a laptop that runs the Bayesian filter for data assimilation in Matlab 2013b. The control commands for the angle of attack are sent out via serial communication to an Arduino UNO that drives the servo. The system parameters identified before the experiments have the same values as listed in Table 1. Figure 7 shows the data stream for the flow-sensing experiment.

Figure 9 presents the measurement data from all six pressure sensors. The data for each sensor has been processed by subtracting the still-water pressure measurement taken before the experiment, in order to eliminate the influence of nonuniform and possibly time-varying bias from the pressure sensors.

Figure 10 shows the time evolution of the marginal probability densities. Observe that the estimated angle of attack α (Fig. 10b) has the same oscillation frequency as the actual angle of attack, with a slightly larger amplitude and a negative phase shift. The estimated camber ratio H (Fig. 10c) has a sinusoidal-like waveform, as predicted in simulation. The estimated relative speed U (Fig. 10a) oscillates around a constant value at double the actuation frequency. The speed oscillation arises from the periodic thrust generated by the flapping motion. The fish robot has the same inertial speed as the uniform flow and consequently exhibits station-holding behavior. (The gantry air tubing and electrical wiring restrict motion of the robot to within the test section.) The average estimated relative flow speed 18.74 cm/s is equal to the incoming uniform flow speed, as observed in Fig. 10a.

Figure 11 shows the moving average of the estimated relative flow speed U . The moving-average window size is equal to one flapping time period. The shaded area shows the standard deviation of the estimate over the corresponding average time window. Note the estimation of the flow speed is more accurate

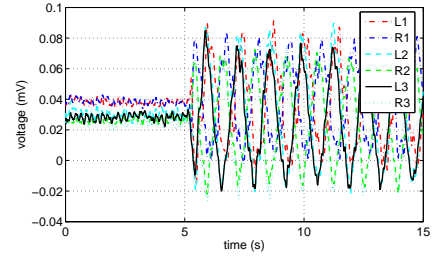


FIGURE 9: The distributed pressure-sensor measurements in the open-loop flow-sensing experiment.

during fish flapping (5 s–15 s) than during fish resting (0 s–5 s), with significant difference in terms of estimation error (5% versus 60%). This observation is contrary to our knowledge of real fish, which may sense the flow better with less turbulence. It is explained by checking the observability Gramian of the robot’s dynamic model with pressure measurements as the system output, which suggests that the flow speed at zero angle of attack is unobservable [9, 10].

CONCLUSION

This paper presents a flow-sensing algorithm using distributed pressure sensors in a flexible fish robot. We design and model a fish robot utilizing the Joukowski transformation to facilitate fluid modeling. We introduce two flow models for the cambered Joukowski-foil-shaped robot, including a quasi-steady potential-flow model for real-time flow estimation and a discrete-time vortex-shedding model for simulating the flow. A recursive Bayesian filter assimilates pressure measurements for estimation of flow parameters. We derive the dynamics of a flexible fish robot and present a reduced model for one-dimensional free swimming. We also present the fabrication of a flexible fish robot and the design of the experimental testbed. The flow-sensing algorithm was tested and validated in both simulation and experiments. In ongoing work, we are investigating a closed-loop control strategy for speed regulation of a flexible fish robot utilizing the estimated flow.

ACKNOWLEDGMENT

This work was supported by the Office of Naval Research under Grant PECASE (No. N000141410249).

REFERENCES

- [1] Tan, X., 2011. “Autonomous robotic fish as mobile sensor platforms: Challenges and potential solutions”. *Marine Technology Society Journal*, **45**(4), pp. 31–40.
- [2] Bandyopadhyay, P. R., 2005. “Trends in biorobotic au-

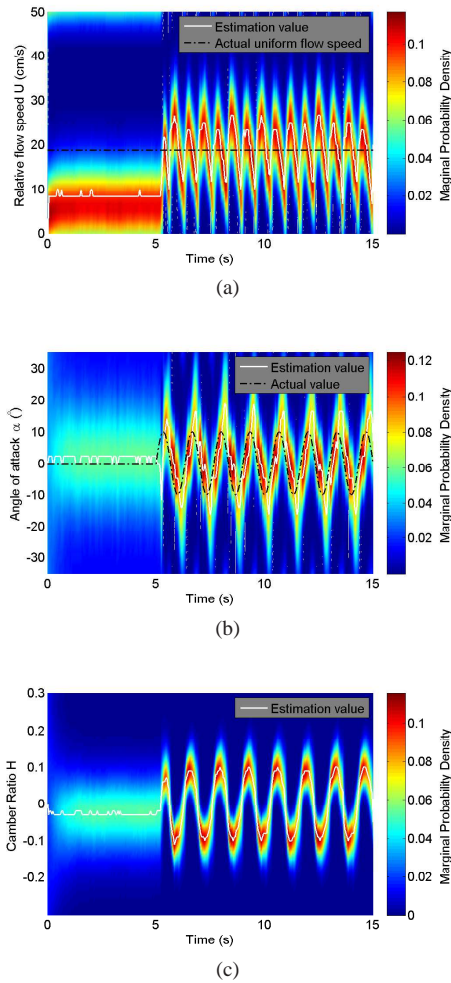


FIGURE 10: Marginal probability density for the states of the Bayesian estimation in the open-loop flow-sensing experiment. (a) the relative flow speed U ; (b) the angle of attack α ; (c) the camber ratio H .

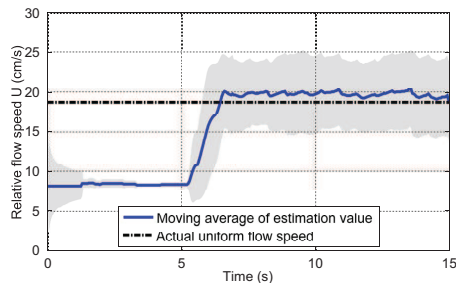


FIGURE 11: The moving average of the estimated relative flow speed U with a window size equal to one flapping time period. Grey area represents \pm one standard deviation of estimated U over the corresponding moving-average time window.

tonomous undersea vehicles”. *IEEE Journal of Oceanic Engineering*, **30**(1), pp. 109–139.

- [3] Kopman, V., and Porfiri, M., 2013. “Design, modeling, and characterization of a miniature robotic fish for research and education in biomimetics and bioinspiration”. *IEEE/ASME Transactions on Mechatronics*, **18**(2), pp. 471–483.
- [4] Morgansen, K. A., Triplett, B. I., and Klein, D. J., 2007. “Geometric methods for modeling and control of free-swimming fin-actuated underwater vehicles”. *IEEE Transactions on Robotics*, **23**(6), pp. 1184–1199.
- [5] Zhang, F., Zhang, F., and Tan, X., 2014. “Tail-enabled spiraling maneuver for gliding robotic fish”. *Journal of Dynamic Systems, Measurement, and Control*, **136**(4), p. 041028.
- [6] Panton, R. L., 2006. *Incompressible flow*. John Wiley & Sons.
- [7] Coombs, S., and Van Netten, S., 2005. “The hydrodynamics and structural mechanics of the lateral line system”. *Fish physiology*, **23**, pp. 103–139.
- [8] Stutters, L., Liu, H., Tiltman, C., and Brown, D. J., 2008. “Navigation technologies for autonomous underwater vehicles”. *IEEE Transactions on Systems, Man, and Cybernetics, Part C: Applications and Reviews*, **38**(4), pp. 581–589.
- [9] Lagor, F. D., DeVries, L. D., Waychoff, K. M., and Paley, D. A., 2013. “Bio-inspired flow sensing and control: Autonomous rheotaxis using distributed pressure measurements”. *Journal of Unmanned System Technology*, **1**(3), pp. 78–88.
- [10] DeVries, L., Lagor, F. D., Lei, H., Tan, X., and Paley, D. A. “Distributed flow estimation and closed-loop control of an underwater vehicle with a multi-modal artificial lateral line”. *Bioinspiration & Biomimetics*. accepted for publication.
- [11] Mason, R. J., 2003. “Fluid locomotion and trajectory planning for shape-changing robots”. PhD thesis, California Institute of Technology.
- [12] Xia, X., and Mohseni, K., 2013. “Lift evaluation of a two-dimensional pitching flat plate”. *Physics of Fluids (1994-present)*, **25**(9), p. 091901.
- [13] Streitlien, K., 1994. “Extracting energy from unsteady flows through vortex control”. PhD thesis, Massachusetts Institute of Technology.
- [14] Holmes, P., Jenkins, J., and Leonard, N. E., 1998. “Dynamics of the kirchhoff equations i: Coincident centers of gravity and buoyancy”. *Physica D: Nonlinear Phenomena*, **118**(3), pp. 311–342.
- [15] Greenwood, D. T., 1988. *Principles of dynamics*. Prentice-Hall Englewood Cliffs, NJ.
- [16] Arulampalam, M. S., Maskell, S., Gordon, N., and Clapp, T., 2002. “A tutorial on particle filters for online nonlinear/non-gaussian bayesian tracking”. *IEEE Transactions on Signal Processing*, **50**(2), pp. 174–188.